Multipredictive Adaptive Control of Arc Welding Trailing Centerline Temperature

T. O. Santos, R. B. Caetano, J. M. Lemos, and F. J. Coito

***Abstract*—This application paper addresses the use of adaptive predictive control on arc welding trailing centerline temperature control. For tackling the high level of uncertainty in the process the multivariable multipredictive adaptive regulator (MUSMAR) adaptive algorithm, relying on separate estimation of predictive models is used. Experimental results presented include characterization of plant uncertainty and of the effect in control performance of various available knobs, in particular in the presence of plates with variable geometry.**

***Index Terms*—Adaptive control, predictive control, process control, welding control.**

I. Introduction

ALTHOUGH automated welding systems have been comercially available for some time, full automation of this process has not yet been achieved because of difficulties concerning control and sensor technologies. Sensor technology problems arise because the main quality related variables are not accessible on-line or are difficult to measure and must be estimated through auxiliary measurements and models [5]. Important contributions have been made for solving these measurement, modeling and control problems of cooling rate and other thermal variables [10], [12]–[14], penetration [9], [15] and weld pool geometry [4], [7], [8], [14]. Sensor and modeling technology aside, the control problem itself presents its own difficulties. This has to do with the fact that the welding process is multivariable, time varying and nonlinear, with significant input–output (I/O) transport delay. For dealing with these difficulties, adaptive control and other algorithms have been adopted in a number of contributions [1], [3], [6], [9], [15], [16].

The purpose of the work reported in this paper is to evaluate the performance of a multivariable multipredictor adaptive regulator (MUSMAR)[18] when used to control thermal characteristics of the welding process. This predictive control algorithm is related to GPC (in the sense that both aim at minimizing a quadratic cost), applied to GTAW in [1], but relies on the separate estimation of a set of predictive models used for computing the manipulated variable value. The redundancy thereby introduced explains the properties of the algorithm when dealing with uncertain plants [19].

As a first step toward cooling rate control, following the line of [11], this paper focuses on trailing centerline temperature control in the gas metal arc welding process. The temperature measurement is achieved by using a commercially available infrared pyrometer with a 3-mm target diameter focused on the trailing weld bead, 2.5 cm from the tip of the electrode (Fig. 1). The manipulated variable is the welding voltage. Wire feed speed is adjusted in conformity with the imposed voltage to ensure a stable electric arc, using the experimental relationship show in Fig. 2. This relationship is valid for the protection gas and electrode used in the experiments (Gas: Ar-CO_2 20–80%. Electrode: Carbon-Steel ϕ 1.2 mm).

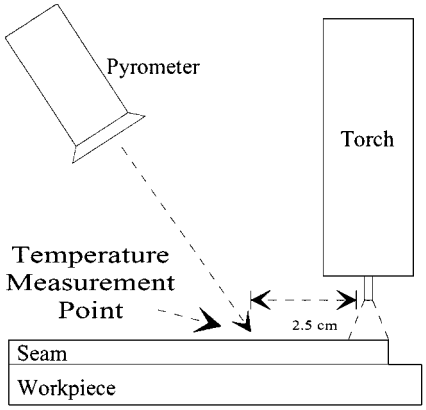

Fig. 1. Trailing centerline temperature measurement.

The main contribution of this paper is the experimental demonstration of the use of the above type of control strategy for improving the performance and robustness of closed-loop welding control. The experimental platform is shown in Fig. 3

II. Process Dynamics

The dynamic behavior of the weld bead centerline temperature is modeled by a set of energy conservation equations describing the energy accumulation in the bead and in the workpiece. The energy propagation is modeled by the heat equation and by heat conduction from the bead to the workpiece. Radiation heat transfer plays a significant role in determining the amount of power delivered and lost by the workpiece. Although these type of models provided significant contributions to the control of the welding process, using both offline and online calibration approaches [2], [4], [5], the difficulties related to the presence of unmodeled dynamics and disturbances have a significant impact on control performance and call for feedback techniques.

Manuscript received April 1, 1997; revised March 10, 1999. Recommended by Associate Editor, R. Middleton.

The authors are with INESC/IST, 1000 Lisboa, Portugal (e-mail: jlml@inesc.pt).

Publisher Item Identifier S 1063-6536(00)00526-1.

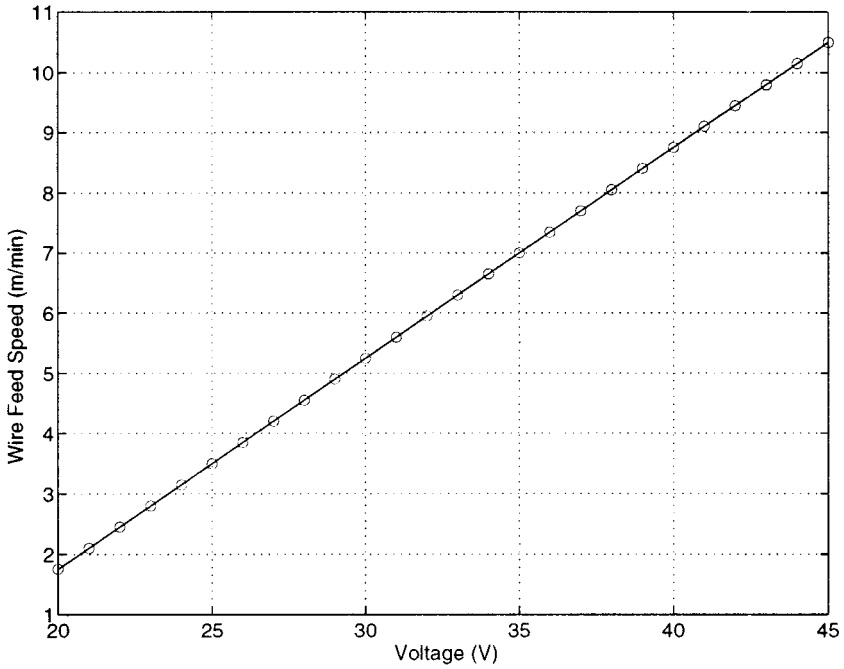

Fig. 2. Experimentally determined relationship between electrode speed and voltage for ensuring a stable arc.

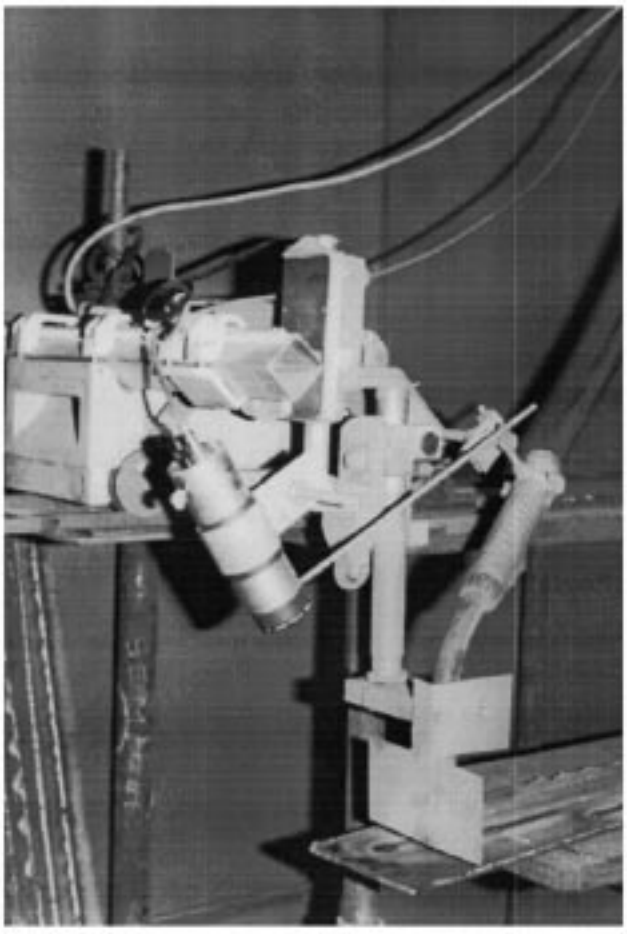

Fig. 3. Experimental platform.

The adaptive control algorithm employed does not rely on an *a priori* model of the process. Nevertheless, experimental identification of the process dynamics provides insight on the difficulties facing control system synthesis, while producing suitable models for simulation based preliminary tests. For this purpose incremental ARMAX models were identified, using open-loop experimental data obtained around several operation points as defined by the input voltage (28, 30, 32, 34, and 36 V) and using different workpiece thicknesses (6 mm and 12 mm). Equation (1) describes the model used, where ΔT and ΔV denote the deviations from the nominal operating point of temperature [°C] and voltage [V], and $e(t)$ stands for a zero mean uncorrelated sequence.The parameters to be identified are a_i, b_i, c_i, for $i = 1, \cdots, n$ being the model order which, after a trial and error process was fixed at $n = 5$. The sampling period for the identification experiments is 200 ms, which corresponds to a sampling frequency $F_s = 5$ Hz

$$\Delta T(t) = \sum_{i=1}^{n} [-a_i \Delta T(t-i) + b_i \Delta V(t-i) + c_i e(t-i)]. \quad (1)$$

The frequency response diagrams of the local ARMAX models obtained using standard system identification software are presented in Figs. 4 and 5 for, respectively, 6- and 12–mm plates. These diagrams are the Bode diagrams [17] of the transfer functions relating the signals ΔV and ΔT around each operating point. These results show the great variability and thereby uncertainty associated with the process.

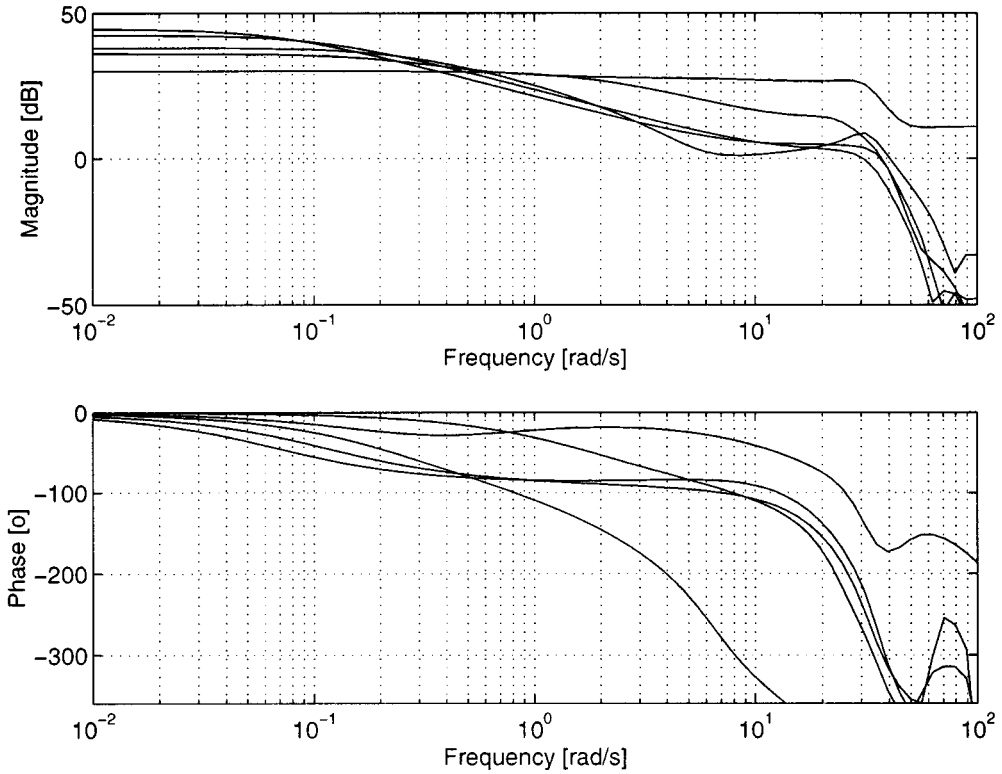

Fig. 4. Bode diagrams of experimental models on a 6-mm plate.

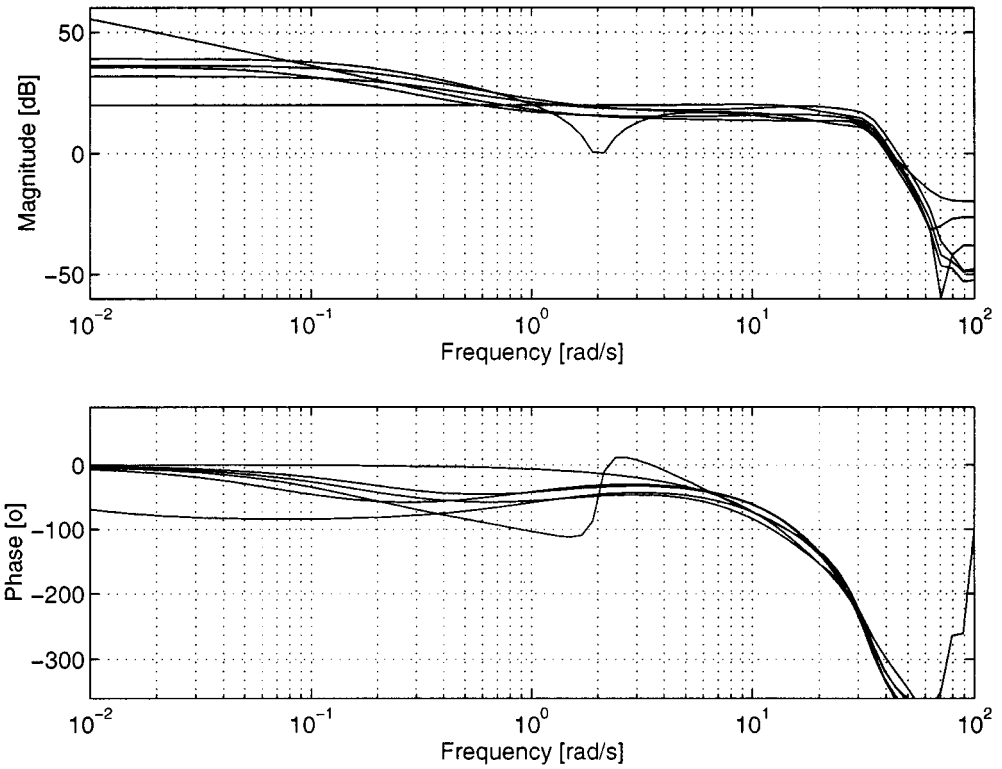

Fig. 5. Bode diagrams of experimental models on a 12-mm plate.

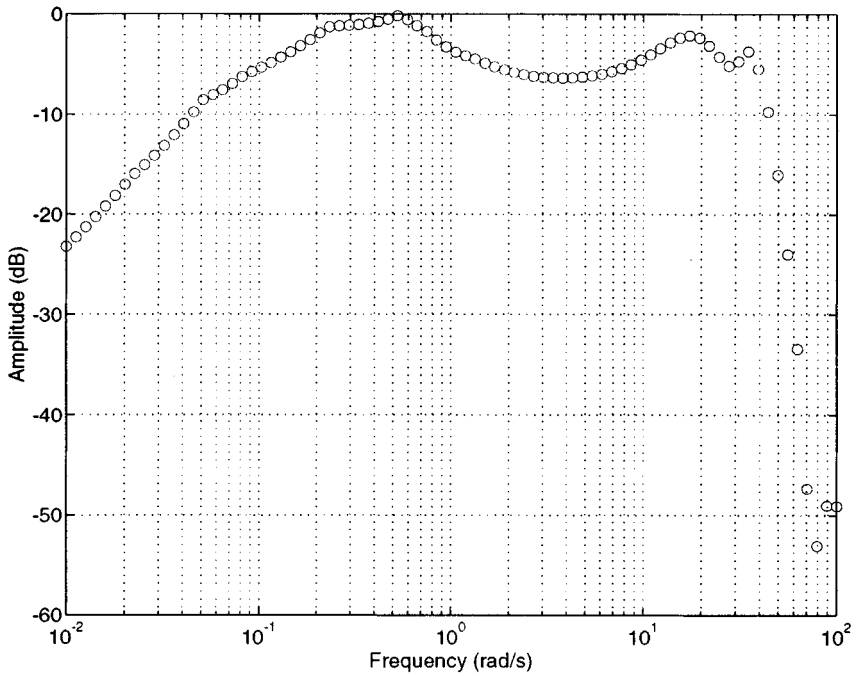

Fig. 6. Inverse magnitude of the process uncertainty.

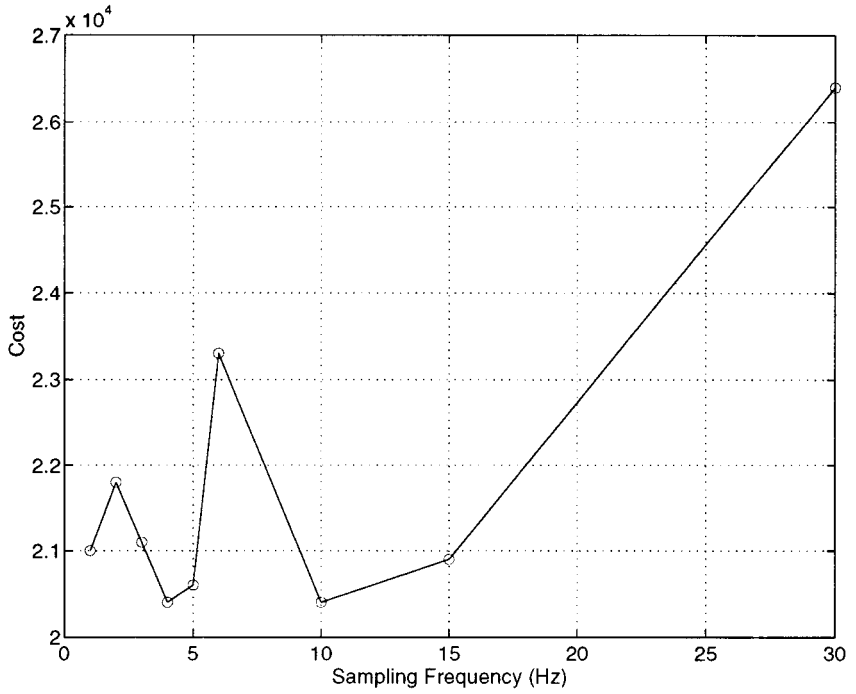

Fig. 7. Dependence of the LQ cost on the sampling frequency F_s.$n_a = 5,\ n_b = 5,\ n_g = 1,\ \lambda = 0.98,\ \rho = 500,\ T = 10$.

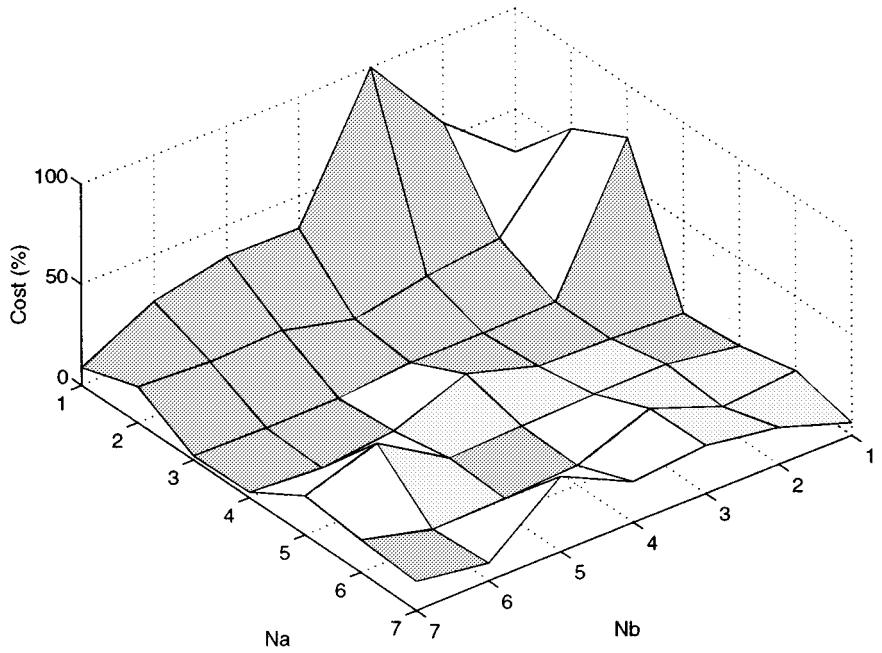

Fig. 8. Dependence of the LQ cost on pseudostate orders. $F_s = 3$ Hz, $n_g = 1$, $\lambda = 0.98$, $\rho = 500$, $T = 10$.

Fig. 6 depicts the envelope diagram of the process uncertainty, relative to an average nominal model. To ensure robust stability in the class of plants considered, the closed-loop transfer function magnitude must be smaller than the inverse of the process uncertainty amplitude [17]. Fig. 6 shows that it is impossible for a fixed gain controller to meet this specification, a fact naturally leading to an adaptive control approach.

In order to get the value of the suitable prediction horizon T, a number of simulations were made. Fig. 9 shows the dependence of the LQ cost with T. A value of $T = 10$ was adopted as convenient.

Fig. 10 shows a simulation of the welding process with the trailing centerline temperature controlled with MUSMAR. The following choices are made: $F_s = 3$ Hz, $T = 10$, $n_a = 3$, $n_b = 3$, $n_g = 1$, $\lambda = 0.98$, $\rho = 1000$. As may be seen, the change of reference does not affect parameter convergence. Offset elimination is discussed below.

III. Adaptive Control

The work reported in Section II motivates the consideration of adaptive control as a way of dealing with the high levels of uncertainty present in this process. The dynamics changes from workpiece to workpiece, being subject to nonlinear and unpredictable time varying effects. Furthermore, a significant I/O transport delay with operating point dependent characteristics is also observed.

A solution based on predictive adaptive control is now considered.

A. Algorithm

The highly correlated noise and disturbances as well as unmodeled dynamics present in the process greatly difficult tuning of an adaptive controller. A class of controllers performing well under these conditions are extended horizon predictive adaptive controllers. Among these, the controller chosen was a multivariable multipredictive adaptive regulator (MUSMAR) [18].

The MUSMAR algorithm is described in the available literature [18], as well as its properties [19]. It suffices here to say that it relies on the minimization of the multistep quadratic cost function

$$J(T) = E\left[\sum_{i=0}^{T-1} y^2(t+i+1) + \rho.u^2(t+i)|I(t)\right] \qquad (2)$$

where

$E[\cdot\|I^t]$	mean conditioned on the set I^t of observations up to time t;
T	integer hereafter referred as the "prediction horizon";
$\rho \geq 0$	penalty in the manipulated variable effort;
u and y	plant manipulated variable (welding voltage in $[V]$) and output (trailing centerline temperature in [°C]).

For the sake of minimizing (2), the plant is described by the set of predictive models

$$\begin{aligned} \hat{y}(t+i|t) &= \theta_i u(t) + \Psi_i' s(t) \\ \hat{u}(t+i-1 \mid t) &= \mu_{i-1} u(t) + \Phi_{i-1}' s(t) \\ i &= 1, \cdots, T \end{aligned} \qquad (3)$$

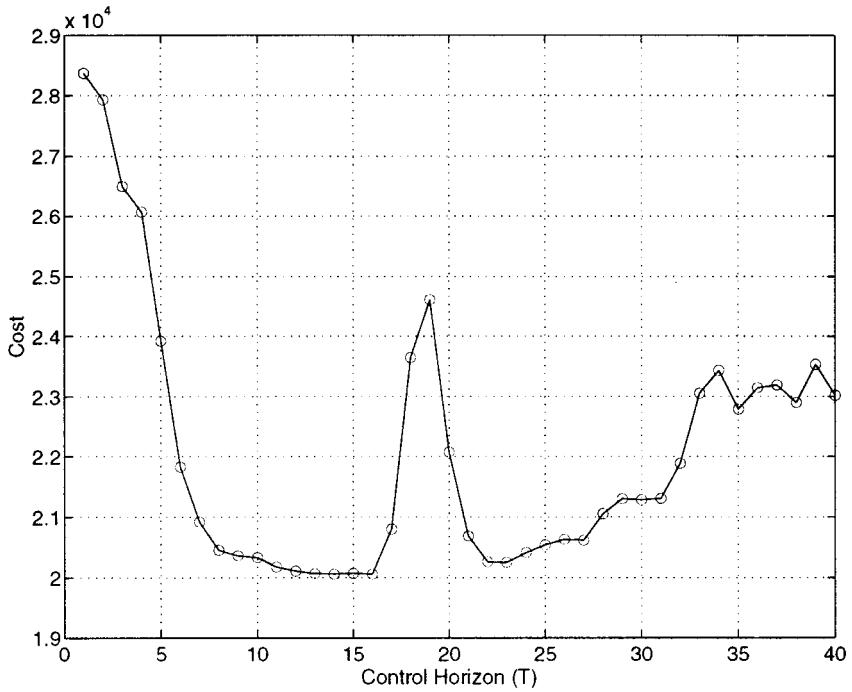

Fig. 9. Dependence of LQ cost on the control horizon T. $F_s = 3$ Hz, $\lambda = 0.98$, $\rho = 500$, $n_a = 3$, $n_b = 3$, $n_g = 1$.

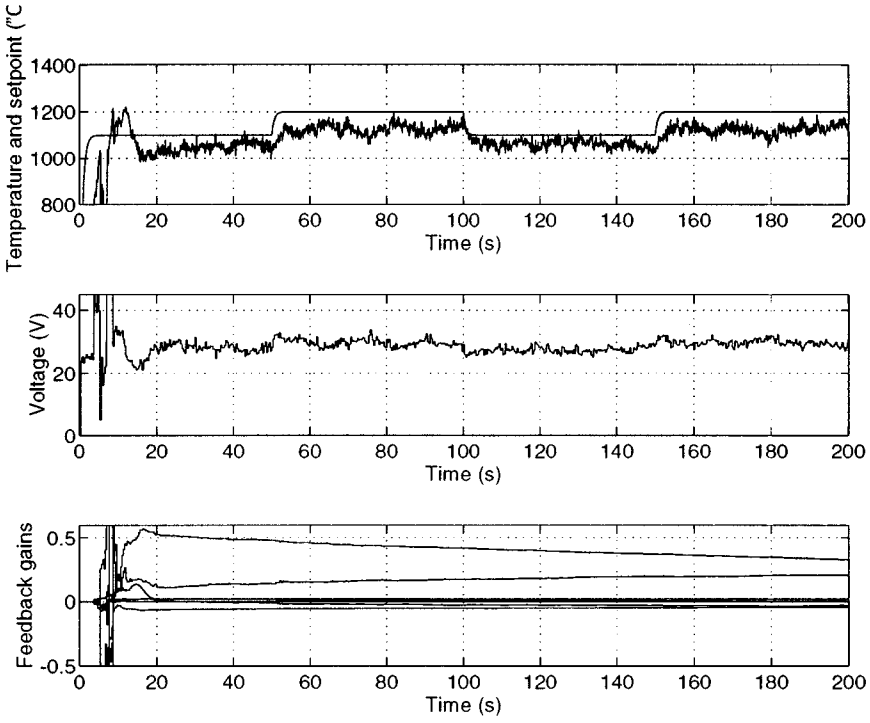

Fig. 10. MUSMAR: Closed-loop simulation. $F_s = 3$ Hz, $T = 10$, $n_a = 3$, $n_b = 3$, $n_g = 1$, $\lambda = 0.98$, $\rho = 1000$, directional forgetting RLS.

where $\hat{y}(t+i|t)$ and $\hat{u}(t+i-1|t)$ are predictors in least squares sense, given I^t of, respectively $y(t+i)$ and $u(t+i-1)$, and $s(t)$ is the so called pseudostate defined by

$$s(t) = [y(t) \cdots y(t-n_a+1)u(t-1) \cdots u(t-n_b)]'. \quad (4)$$

The vector $s(t)$ is called "pseudostate" [18], [19] because, even in the presence of correlated noise, although it is not a state, it is a sufficient statistic for computing the control. The entries of $s(t)$ define the structure of the controller. In addition to samples of the input and output variables, samples of other variables such

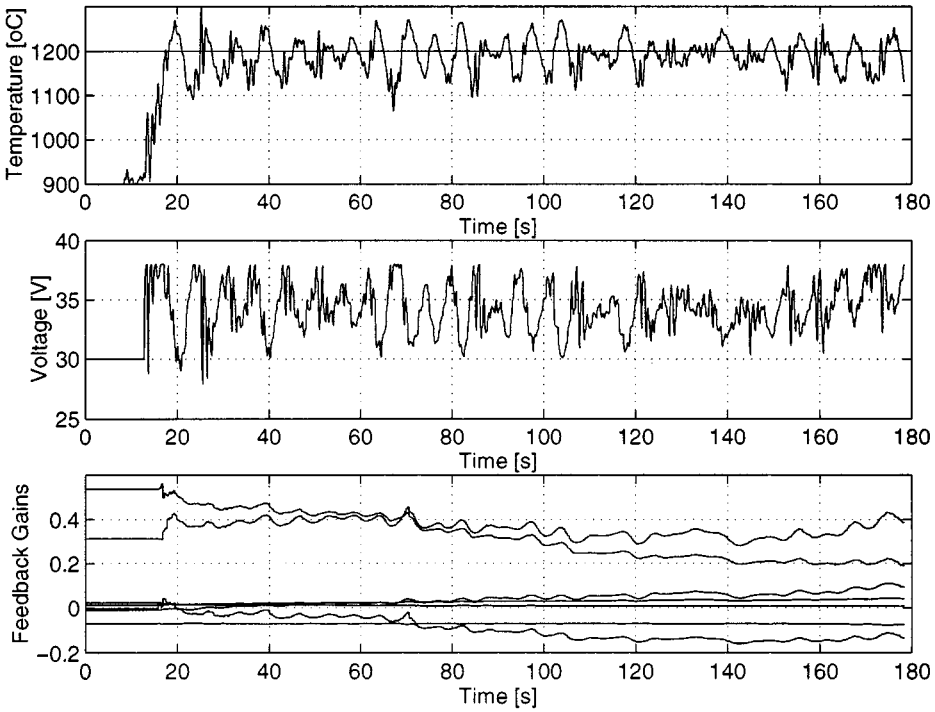

Fig. 11. Experimental plant behavior under closed-loop control. $F_s = 3$ Hz, $\lambda = 0.98$, $\rho = 100$, directional forgetting RLS. $1/(T = 10,\ N_a = 3N_b = 3,\ N_g = 1)$

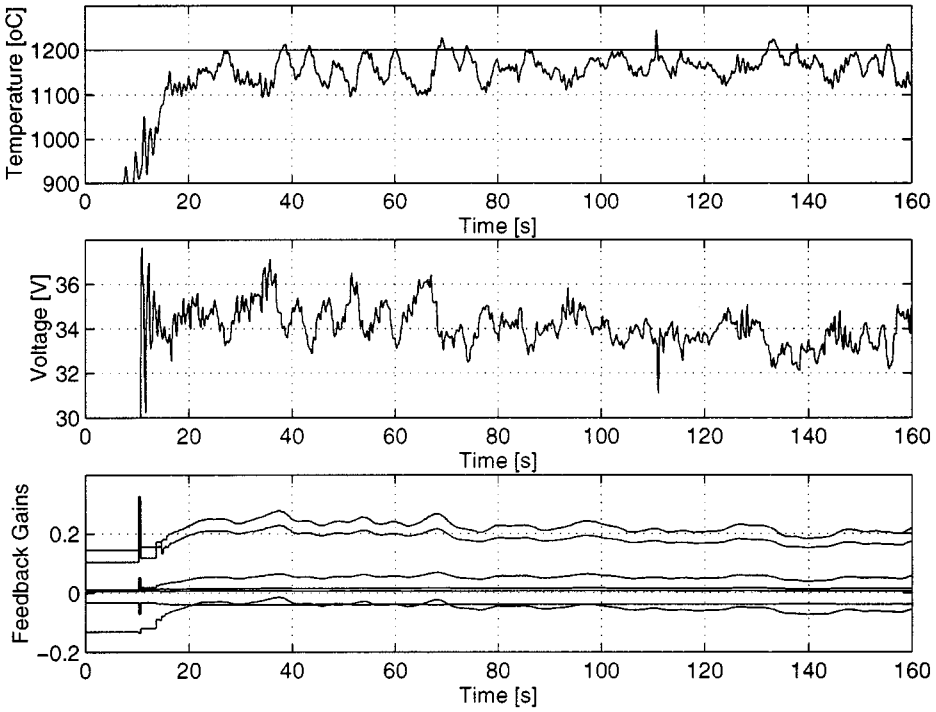

Fig. 12 Experimental plant behavior under closed-loop control. $F_s = 3$ Hz, $T = 10$, $n_a = 3$, $n_b = 3$, $n_g = 1$, $\lambda = 0.98$, $\rho = 1000$, directional forgetting RLS.

as accessible disturbances may also be included. In order to provide a feedforward effect from the reference to track, samples of this variable are also included in $s(t)$, the number of these samples being denoted n_g. Usually, since the reference is constant most of the time, in order to prevent identifiability problems, the choice $n_g = 1$ is made.

Offset compensation by introduction of parallel integration allows increasing the control weight to ensure a more regular

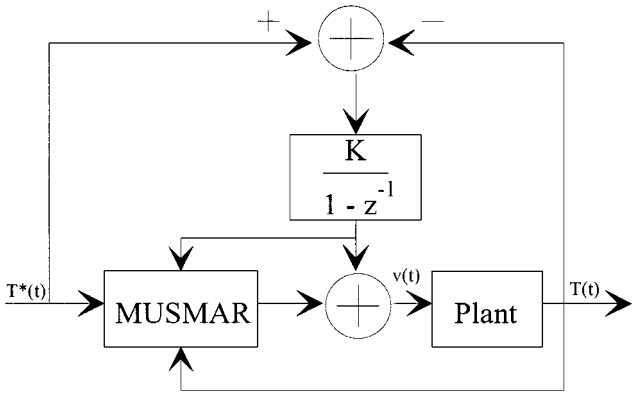

Fig. 13. Diagram of parallel integration ($K = 7 \times 10^{-5}$).

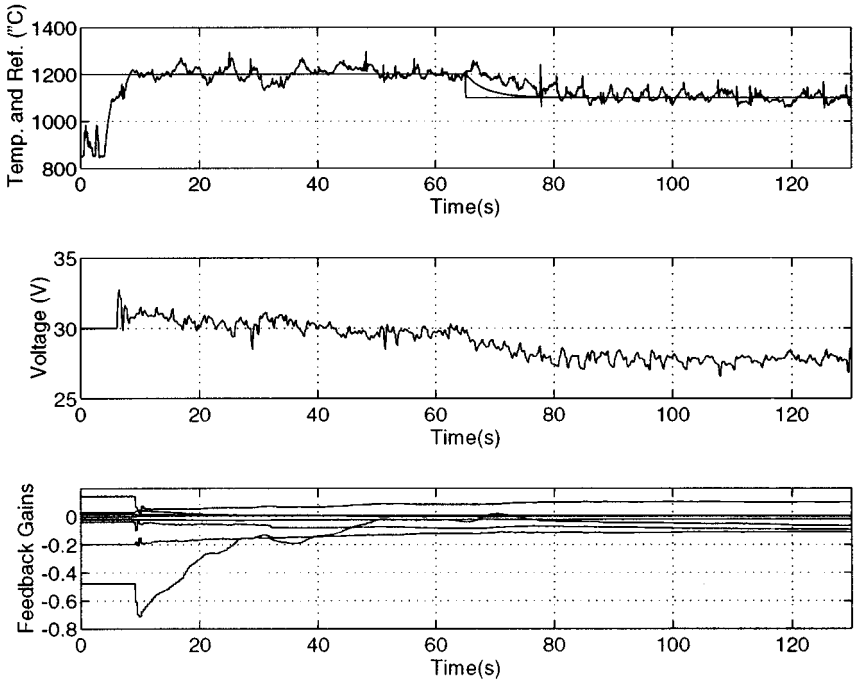

Fig. 14. Experimental plant behavior under closed-loop control with parallel integration. 12 mm plate, $F_s = 3$ Hz, $\rho = 2000, T = 10, n_a = 3, n_b = 3, n_g = 1, n_v = 1$.

welding seam. Fig. 14 shows the performance of the control system with increase control weight ($\rho = 2000$) and Fig. 15 depicts the resulting weld seam. These results show that the temperature reference was tracked and the weld seam has stayed reasonably regular.

The coefficients θ_i, μ_{i-1}, and vectors Ψ_i, Φ_{i-1} in (3) are parameters to be estimated online. These parameters have no physical meaning, being regression coefficients which reflect the mutual dependence among the variables. For each i, $i = 1, \cdots, T$, this set of parameters describes the dynamic behavior of the process output and manipulated variable from t to $t + i$, assuming a constant feedback of the pseudostate over the prediction horizon [18]. Minimization of (2) assuming (3) yields the control law

$$u(t) = L's(t) + \eta(t) \tag{5}$$

Fig. 15. Seam of the test of Fig. 15.

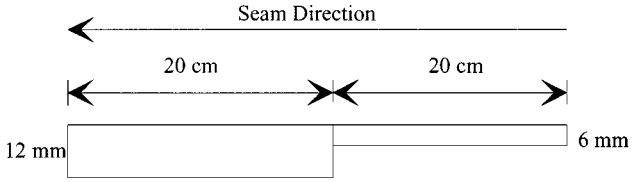

Fig. 16. Side view of the work piece of experiment I.

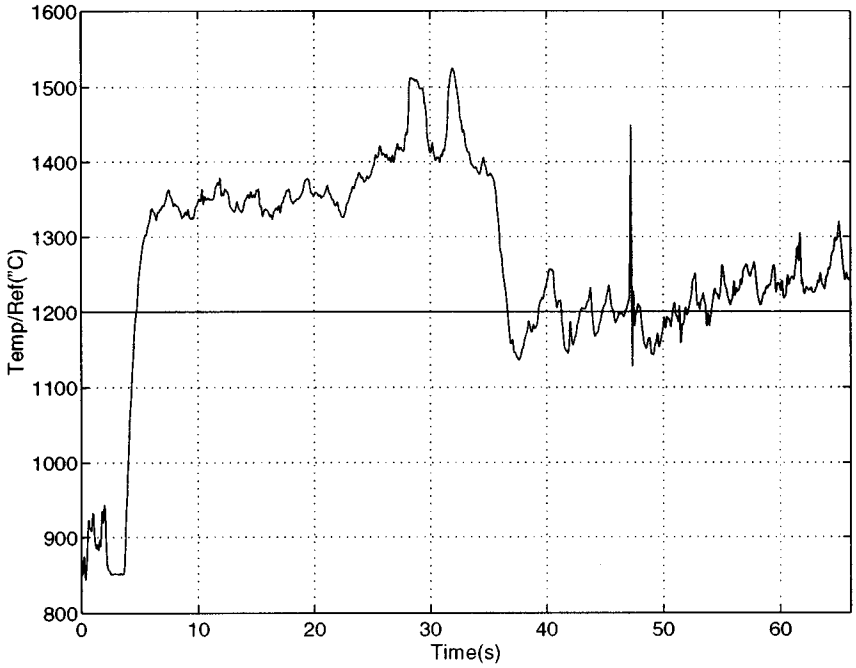

Fig. 17. Trailing centerline temperature behavior without control.

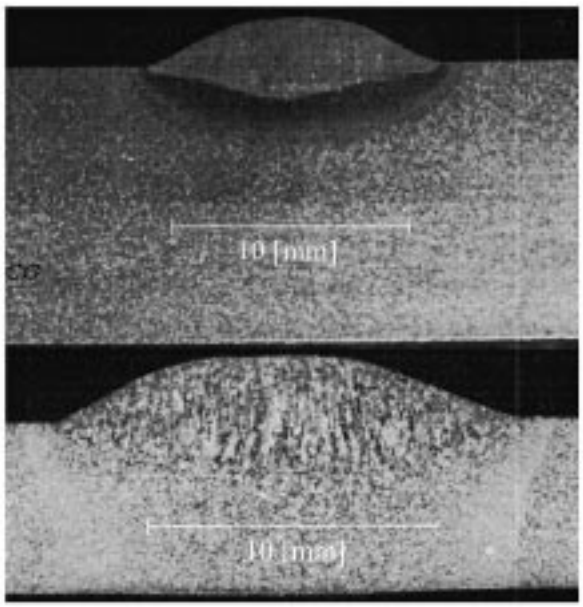

Fig. 18. Cross sections of the plates without feedback control. Top: 12-mm plate. Bottom: 6-mm plate.

with the vector of optimal gains given by

$$L = -\frac{\sum_{i=1}^{T} \theta_i \Psi_i + \rho \sum_{i=1}^{T-1} \mu_i \Phi_i}{\sum_{i=1}^{T} \theta_i^2 + \rho \left(1 + \sum_{i=1}^{T-1} \mu_i^2\right)}. \tag{6}$$

The identification algorithm used was recursive least squares with directional forgetting factor [20]. This algorithm was chosen because weld is a regulation problem, and when all the transient responses are extinguished the standard algorithm with exponential forgetting factor [17] loses past information about the plant in a way possibly causing bursts. The forgetting factor coefficient is denoted λ.

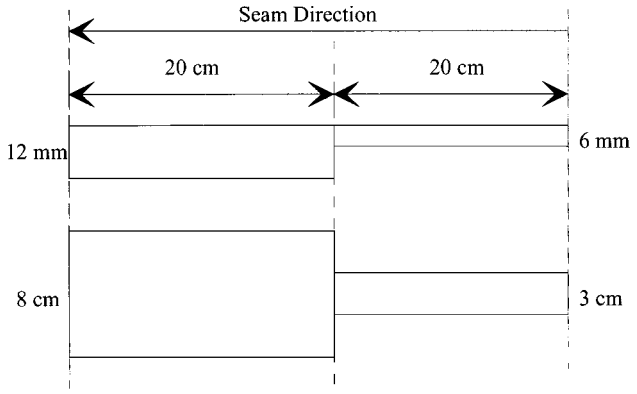

Fig. 19. Work piece of experiment II.

B. Controller Structure

The adjustment of the controller parameters must take into account the compromise between the control signal (voltage) oscillation and temperature setpoint tracking. This compromise is achieved by adjusting the control weighting penalty parameter ρ. Before tuning this parameter it is necessary to guarantee the performance of the identification algorithm, and to get an estimate of the best orders for the controller. This was achieved by simulation. The tuning of ρ was performed experimentally.

To get an initial estimate of the suitable range of values for the parameters defining controller structure (T, n_a, n_b, λ, ρ, sampling frequency F_s), the identified models were used for evaluating the adaptive controller performance under a number

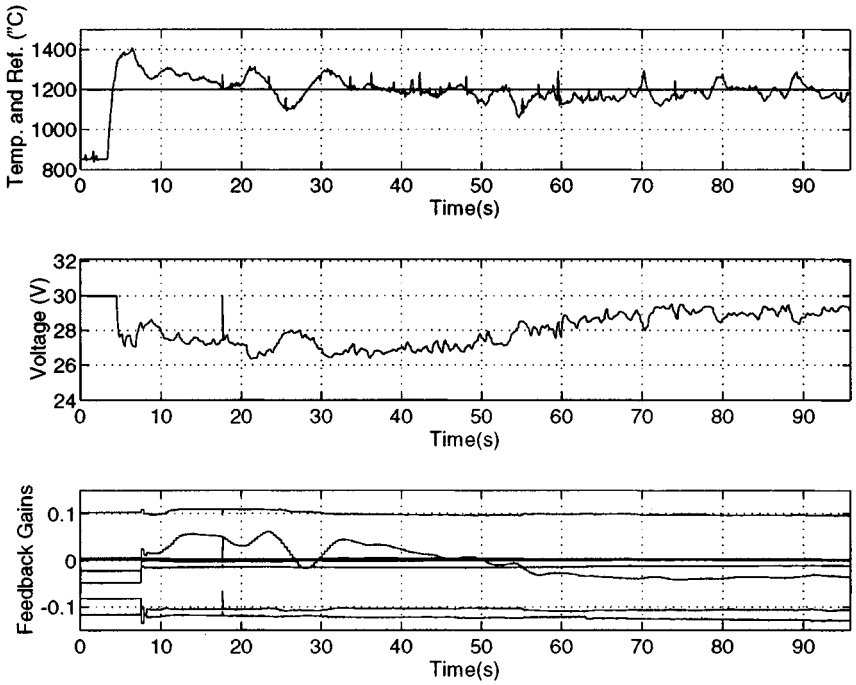

Fig. 20. Plant behavior under closed-loop control. $T = 10$, $n_a = 3$, $n_b = 3$, $n_g = 1$, $\rho = 2000$, with parallel integrator and $n_v = 1$.

Fig. 21. Detail of the weld seam of experiment II.

of different conditions. The initially assumed model orders were those of the experimentally identified ARMAX models ($na = 5,\ nb = 5$). A latter evaluation of control performance with different values of the sampling frequency showed that a larger sampling period was more convenient ($F_s = 3$ Hz, see Fig. 7) and the optimal model orders could be reduced to $n_a = 3, n_b = 3$ (Fig. 8).

C. Integral Effect

Experimental plant behavior under MUSMAR closed-loop control with low control penalty ($\rho = 100$) is presented in Fig. 11. Under these conditions the voltage oscillation yields an irregular weld seam as a result of poor temperature regulation.

For the sake of reducing the undesirable oscillation on the control signal observed in Fig. 11, the value of the penalty ρ in (2) must be increase. The corresponding experimental result is presented in Fig. 12. However, a steady-state position error in the temperature is observed due to the increase in the control signal penalty ρ. For rejecting this error the preferred solution was parallel integration with a small constant gain K (Fig. 13). The inclusion of a parallel instead of a series integrator has the advantage of reducing the interference with the adaptive algorithm.

The increase in plant order due to the parallel integrator suggests introduction of its output into the pseudostate vector $s(t)$. Thus, one term of the compensation signal was introduced in the pseudostate (hereafter taken as $n_v = 1$).

D. Plates with Varying Geometry

The purpose of the work reported in this section is to illustrate the performance of the control system on the presence of plates with variable geometry as well as its effect on some of the weld seam resulting characteristics.

Experiment I—Open-Loop: This experiment was designed to evaluate the effect of varying geometry on open-loop welding. Fig. 16 shows the thickness profile of the plate used. The plate width is constant (8 cm).

Fig. 17 shows the time evolution of the temperature. This provides an image of the temperature behavior along the weld seam. When the weld pool is on the 6-mm plate, the trailing centerline temperature is about 200°C higher than that of the 12-mm plate. Fig. 18 shows a cross section of the thermally affected zone of the thin and thick plates. While on the thin plate (Fig. 18, bottom) there is significant overheating, on the thick plate (Fig. 18, top) there is poor penetration.

Experiment II—Controlled: This experiment is the equivalent of the previous one, under closed-loop control. To create a greater variation on the process, both the thickness and the width of the plate change simultaneously (Fig. 19).

Fig. 20 shows the temperature behavior under closed-loop control. The disturbance introduced by the variation of geometry was reduced. The weld seam stayed reasonably regular (Fig. 21), and the thermally affected zones of the plate show a higher penetration in the thick plate (Fig. 22, top) and much reduced overheating in the thin plate (Fig. 22, bottom).

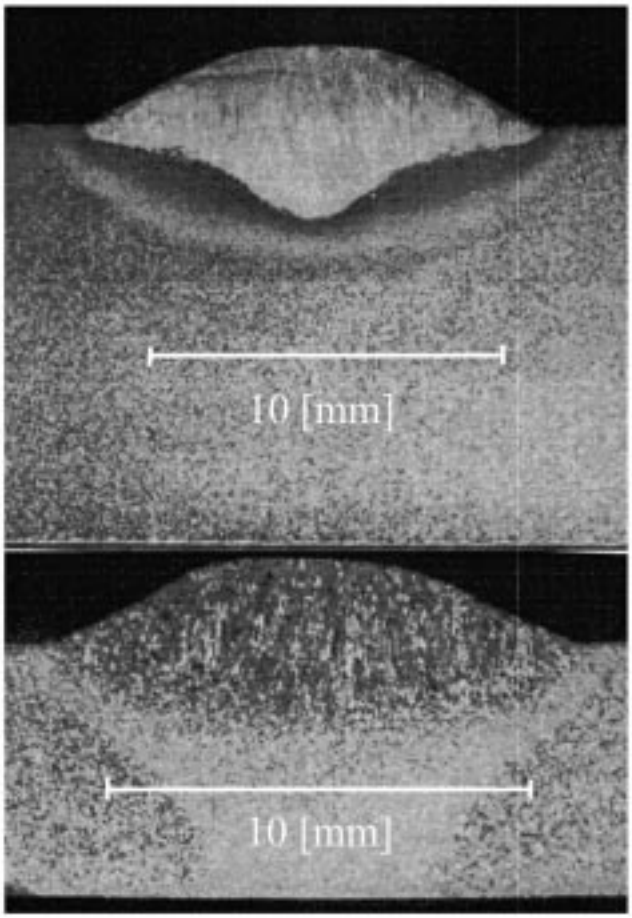

Fig. 22. Cross sections of the plates with feedback control. Top: 12-mm plate. Bottom: 6-mm plate.

IV. Conclusions

The high level of uncertainty due to the variability of dynamics of arc welding trailing centerline temperature pose difficulties to control when using a constant linear controller. It is thus a natural example for application of adaptive control. The predictive adaptive controller MUSMAR was applied, the dependence on its configuring parameters being documented.

In the experiments shown, a reasonable compromise is achieved between the regularity of the weld seam and trailing centerline temperature regulation. The importance of closed-loop control is illustrated in the last section where, in extreme changes of the workpiece geometric configuration, the resulting weld seam properties became more homogeneous than those corresponding to open-loop welding. It is stressed, however, that penetration is not being controlled.

References

[1] R. Kovasevic, Y. M. Zhang, and S. Ruan, "Sensing and control of weld pool geometry for automated GTA welding," *Trans. ASME J. Eng. Ind.*, vol. 117, no. 2, pp. 210–222, May 1995.

[2] C. C. Doumanidis, "Multiplexed and distributed control of automated welding," *IEEE Contr. Syst. Mag.*, vol. 14, no. 4, pp. 13–24, Aug. 1994.

[3] J. B. Song and D. E. Hardt, "Dynamic modeling and adaptive control of the gas metal arc welding process," *Trans. ASME J. Dynamic Syst. Measurement Contr.*, vol. 116, no. 3, pp. 405–413, Sept. 1994.

[4] D. E. Hardt, D. A. Garlow, and J. B. Weinert, "A model of full penetration arc welding for control system design," *Trans. ASME J. Dynamic Syst. Measurement Contr.*, vol. 107, pp. 40–46, Mar. 1985.

[5] B. E. Bates and D. E. Hardt, "A real-time calibrated thermal model for closed-loop weld bead geometry control," *Trans. ASME J. Dynamic Syst. Measurement Contr.*, pp. 25–33, Mar. 1985.

[6] A. Suzuki, D. E. Hardt, and L. Valavani, "Application of adaptive control theory to on-line GTA weld geometry regulation," *Trans. ASME J. Dynamic Syst. Measurement Contr.*, pp. 93–103, Mar. 1991.

[7] R. Masmudi and D. E. Hardt, "Multivariable control of geometric and thermal properties in GTAW," presented at the 3rd ASM Conference Trends Welding Research, Gatlinburg, TN, June 1992.

[8] J. B. Song and D. E. Hardt, "Multivariable control of bead geometry in GMA welding," presented at the ASME WAM Symposium Welding, Dec. 1991.

[9] Y. M. Zhang, R. Kovacevic, and L. Li, "Adaptive control of full penetration gas tungsten arc welding," *IEEE Trans. Cont. Sys. Technol.*, vol. 4, July 1996.

[10] C. C. Doumanidis and D. E. Hardt, "Simultaneous in-process control of heat affected zone and cooling rate during arc welding," *Welding J.*, vol. 69, no. 5, pp. 186s–196s, May 1990.

[11] D. V. Nishar, J. L. Schiano, W .R. Perkins, and R. A. Weber, "Adaptive control of temperature in arc welding," *IEEE Contr. Syst. Mag.*, pp. 4–12, Aug. 1994.

[12] D. V. Nishar, "Feedback control of bead temperature in gas metal arc welding,", Rep. DC-142, UILU-ENG-92-2231, Aug. 1992.

[13] K. E. Dorschu, "Control of cooling rates in steel weld metal," *Welding J. Res. Suppl.*, vol. 47, no. 2, pp. 49–68, 1968.

[14] J. L. Schiano, D. E. Henderson, J. H. Ross, and R.A. Weber, "Image analysis of puddle geometry and cooling rate for gas metal arc welding control," in *Proc. Int. Soc. Opt. Eng., Midwest Tech. Conf.*, Chicago, IL, 1990.

[15] R. Kovasevic and Y. M. Zhang, "Neurofuzzy model-based weld fusion state estimation," *IEEE Contr. Syst. Mag.*, vol. 17, no. 2, pp. 30–42, Apr. 1997.

[16] L. J. Brown, S. P. Meyn, and R. A. Weber, "Adaptive dead-time compensation with application to a robotic welding system," *IEEE Trans. Contr. Syst. Technol.*, vol. 6, no. 3, pp. 335–349, May 1998.

[17] K. J. Åstrom and B. Wittenmark, *Computer-Controlled Systems*. Englewood Cliffs, NJ: Prentice-Hall, 1997.

[18] C. Greco, G. Menga, E. Mosca, and G. Zappa, "Performance improvements of self-tuning controllers by multistep horizons: The MUSMAR approach," *Automatica*, vol. 20, pp. 681–699, 1984.

[19] E. Mosca, G. Zappa, and J. M. Lemos, "Robustness of multipredictor adaptive regulators: MUSMAR," *Automatica*, vol. 25, pp. 521–529, 1989.

[20] R. Kulhavy, "Restricted exponencial forgetting in real-time identification," *Automatica*, vol. 23, pp. 589–600, 1987.